CHEMICAL ENGINEERING TRANSACTIONS
VOL. 120, 2025
A publication of AIDIC
The Italian Association of Chemical Engineering
Online at www.cetjournal.it
Guest Editors: Bing Shen How, Viknesh Andiappan, Denny K.S. Ng, Hon Loong Lam, Petar S. Varbanov

ISBN 979-12-81206-21-2; **ISSN** 2283-9216
DOI: 10.3303/CET25120050

The Effect of Fluid Velocity on the Performance of Evacuated Solar Thermal Collectors Under Scaling Conditions

Hebert G. Lugo-Granados[a,*], Lázaro Canizalez-Dávalos[a], Martín Picón-Núñez[b]

[a]Autonomous University of Zacatecas, Department of Chemical Engineering, Zacatecas, México
[b]University of Guanajuato, Department of Chemical Engineering, Guanajuato, Gto., Mexico
lugh871024@gmail.com

The performance of solar collector networks decreases due to scaling fouling caused by the accumulation of calcium carbonate ($CaCO_3$), which reduces thermal efficiency and increases the system pressure drop. This study analyses the impact of flow velocity on the outlet temperature and pressure drop in evacuated flat-plate solar collectors across different operating times. The results indicate that, with a flow velocity of 4 m/s, scaling fouling increases the number of collectors required to reach the target temperature by 12 %. In contrast, with a velocity of 0.15 m/s, the collectors increase by 5 %. Operating at higher flow velocities helps mitigate fouling, resulting in a minor reduction in the outlet temperature. On the other hand, lower flow velocities promote the accumulation of deposits and accelerate the loss of thermal efficiency. The analysis found that the pressure drop increases due to three main factors: fouling caused by scaling, the installation of collectors in series, especially when exceeding ten collectors and extended operating periods of the solar network (t > 2,160 h). The results showed that it is necessary to improve flow distribution to ensure good performance and extend the lifespan of solar collector networks under fouling conditions.

1. Introduction

Evacuated flat-plate solar collectors represent an efficient solution for harnessing solar thermal energy in various applications, especially in industrial processes requiring medium temperatures between 120 and 180 °C (Gao et al., 2020). Evacuated flat-plate collectors (EFPC) combine the design of traditional flat-plate collectors (FPC) with the vacuum principle of evacuated tube collectors (ETC). The collector vacuum system minimises convective heat losses, enhancing thermal efficiency and reducing space requirements compared to ETCS (Carrión-Chamba et al., 2022). However, their performance can be affected by the accumulation of mineral deposits ($CaCO_3$). This phenomenon, known as scaling, reduces thermal efficiency and increases the system's hydraulic resistance, negatively impacting its long-term performance.

Several numerical studies have evaluated the thermal performance of different types of thermal solar collectors. Albizzati (2016) conducted a comparative analysis between flat-plate collectors (FPC) and evacuated tube collectors (ETC). This study demonstrated that FPCs exhibit lower thermal efficiency (34 %), while ETCs achieve values from 46.3%. Bellos et al. (2023) analyzed an EFPC operating below 200 °C and developed a correlation to estimate daily useful energy output based on operating temperature, solar irradiation, and ambient temperature. They found that the optimal exergy and thermal efficiencies were 13.33 % and 47.24 % at 125 °C, with energy and exergy costs of €0.0274/kWh and €0.1043/kWh. In parallel, computational studies have focused on modeling the thermal and hydraulic behavior of solar collectors. Nedunchezhiyan et al. (2023) employed numerical simulations to analyze hybrid evacuated tube and flat plate solar collectors, examining the impact of different flow rates on velocity, pressure, temperature, and turbulent kinetic energy. Their findings indicate that a flow rate of 1 L/min maximizes thermal efficiency (68.5 %). Additionally, Haghverdi et al. (2023) developed a CFD model for a polycarbonate flat plate solar collector, validating their numerical results against experimental data, which enabled design optimization and cost analysis. However, these studies do not account for the effects of scaling fouling, a limitation that affects their long-term applicability.

Paper Received: 10 May 2025; Revised: 11 August 2025; Accepted: 7 September 2025
Please cite this article as: Lugo-Granados H.G., Canizalez Dávalos L., Picón-Núñez M., 2025, The Effect of Fluid Velocity on the Performance of Evacuated Solar Thermal Collectors Under Scaling Conditions, Chemical Engineering Transactions, 120, 295-300 DOI:10.3303/CET25120050

In recent studies, Lugo-Granados et al. (2023) focused their research on the impacts of scaling fouling on the instantaneous thermohydraulic performance of solar collector fields. In a subsequent study, Lugo-Granados et al. (2024) determined that the optimal design of a flat-plate solar collector network in continuous operation can generate annual savings of $ 17,523 under clean conditions and $ 19,819 under fouling conditions, compared to the operational cost of using natural gas. They evaluated various network arrangements to maximize production in a batch process, considering the impact of scaling fouling on system performance.
This study analyses how scaling accumulation can intensify in solar collectors operating at reduced flow velocities, especially due to inefficient fluid distribution. It also demonstrates that poor flow distribution not only affects the system thermal efficiency but also contributes to increased fouling, negatively impacting the lifespan and overall performance of the solar collector.

2. Methodology

For the analysis of evacuated flat-plate solar collectors, a thermal model is derived from the one used for conventional collectors. These systems have the advantage that the vacuum acts as an excellent thermal insulator. This significantly reduces energy losses through convection, improving heat retention and increasing the system efficiency. Figure 1 illustrates the components of an evacuated flat-plate collector, which consists of an aluminum housing serving as the main structure. Additionally, it includes a glass cover, an absorber plate, copper tubes for heat exchange, and a lower plate, which together optimize the capture and transfer of thermal energy.

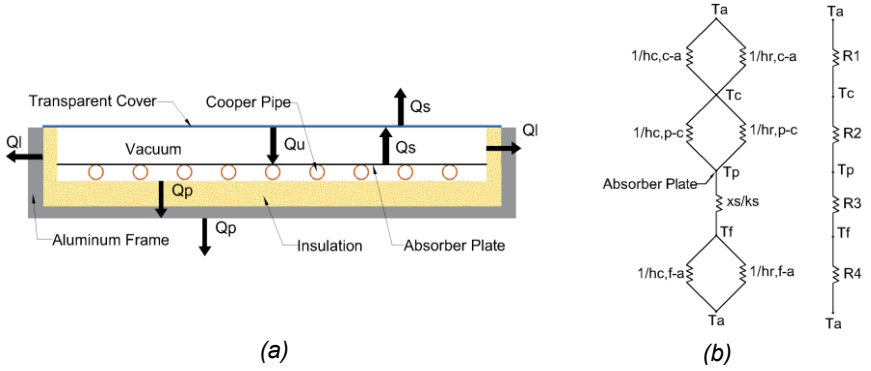

Figure 1: a) Vacuum flat plate collector components, b) Heat transfer resistances within the solar system

The heat flow absorbed by the collectors Eq(1), denoted as $\dot{Q}_u$ (W), is determined by the heat removal factor (F_R), the collector area As (m^2), solar radiation I_G (W/m^2), the overall heat loss coefficient Uc ($W/(m^2\ °C)$), the temperature difference between the absorber plate (Tp-Ta) (°C), and the absorptance (αc) and transmittance (τ) of the cover.

$$\dot{Q}_u = F_R A_s \left[I_G(\tau\alpha_c) - U_c(T_p - T_a) \right] \quad (1)$$

Figure 2 illustrates the thermal model representing the relationship between the absorber plate temperature T_{pm} (°C) and the ambient temperature T_a (°C). The overall heat loss coefficient U_C ($W/(m^2\ °C)$) combines three components: the top loss coefficient U_s ($W/(m^2\ °C)$), the back loss coefficient U_P ($W/(m^2\ °C)$), and the side loss coefficient U_l ($W/m^2°C$), as shown in Eq(2).

$$U_c = U_s + U_p + U_l \quad (2)$$

The top heat loss coefficient (U_S) is defined as the inverse of the sum of the thermal resistances R_1 ($m^2\ °C/W$) and R_2 ($m^2\ °C/W$) within the collector as indicated in Eq(3). Thermal resistance R_1 (Eq(4)) accounts for heat transfer via convection (hc_{c-a} ($W/(m^2\ °C)$)) and radiation (hr_{c-a} ($W/(m^2\ °C)$)) between the absorber plate and the environment. Resistance R_2 (Eq(5)) corresponds to the region between the plate and the cover.

$$U_s = \frac{1}{R_1 + R_2} \quad (3)$$

$$R_1 = \frac{1}{hr_{c-a} + hc_{c-a}} \quad (4)$$

$$R_2 = \frac{1}{hr_{p-c}} \tag{5}$$

The back loss coefficient (U_p) depends on thermal resistances from conduction through the insulation (R_3 (m^2 °C/W)) and from combined convection and radiation (R_4 (m^2 °C/W)) between the backplate and the surroundings, Eq(6). (R_4) is negligible compared to (R_3), (Eq (7)). Here, k_s is the thermal conductivity and x_s is the thickness of the back insulation material.

$$U_p = \frac{1}{R_3 + R_4} \tag{6}$$

$$R_3 = \frac{k_s}{x_s} \tag{7}$$

The side heat loss coefficient (U_l) is derived considering one-dimensional thermal flux across the perimeter and area (A_c) collector, as shown in Eq(8). Where x_l is the side insulation thickness, p and h are the perimeter and the hight of the collector.

$$U_l = \left(\frac{k_s}{x_l}\right) \cdot \left(\frac{p\,h}{A_c}\right) \tag{8}$$

The heat removal factor, Eq(9), is a function of the mass flow rate $\dot{m}_f$ (kg/s), and the efficiency factor of the collector. The term F´ in Eq(10) is a function of the tube spacing S (m), the inner diameter d_i (m) and outer diameter d_o (m) of the tubes, and the heat transfer resistances from the absorber plate to the working fluid. It also includes the resistance arising from convection between the inner tube wall and the working fluid R_h (m^2 °C/W). The resistance due to the tube wall R_t (m^2 °C/W) and the fouling layer resistance R_s (m^2 °C/W). C_b (m^2 °C/W) is the resistance caused by the tube/plate bond and is described in Eq(11).

$$F_{R,\theta} = \frac{\dot{m}_f Cp_f}{A_s\, U_c}\left[1 - e^{\frac{-A_s\, U_c F'}{\dot{m}_f Cp_f}}\right] \tag{9}$$

$$F' = \frac{1/U_{c,\theta}}{S\left[\frac{1}{U_{c,\theta}\left[d_0 + F_{A,\theta}(S - d_0)\right]} + \frac{1}{C_{b,\theta}} + \frac{R_{h,\theta}}{\pi d_s} + \frac{R_{t,\theta}}{\pi d_s} + \frac{R_{s,\theta}}{\pi d_s}\right]} \tag{10}$$

$$C_{b,\theta} = k_b W/\gamma \tag{11}$$

where kb (W/(m °C)) is the thermal conductivity of the junction, W (m) is the width, and γ (m) is the thickness of the junction between the plate and the tube. Eq(12) is described by the hydraulic diameter ds (m), and xf (m) is the thickness by scaling.

$$d_s = d_i - 2x_f \tag{12}$$

Additionally, F´ depends on the thermal efficiency of the metal fin (F_A) as given by Eq(13).

$$F_A = \frac{Tanh[M_\theta(S - d_0)/2]}{M_\theta(S - d_0)/2} \tag{13}$$

$$M_\theta = \sqrt{(U_{c,\theta}/(k_{p,\theta})\delta)} \tag{14}$$

The terms k_p (W/m °C) and δ (m) represent the thermal conductivity and plate thickness, and the parameter M (m^{-1}), is defined in Eq(14). The fouling thermal resistance, R_s (m^2 °C/W), is a function of the mass flux of $CaCO_3$ deposited on the tubes, denoted as $\dot{m}_d$ (kg/(m^2 s)), mass flux being removed, $\dot{m}_r$ (kg/(m^2 s)), the density ρ_f (kg/m^3), and the thermal conductivity λ_f (W/m °C) of $CaCO_3$, Eq(15).

$$\frac{dR_{s,\theta}}{dt_{,\theta}} = \frac{\dot{m}_{d,\theta} - \dot{m}_{r,\theta}}{\rho_{f,\theta}\lambda_{f,\theta}} \tag{15}$$

To determine the amount of scaling ($CaCO_3$) deposited on the inner collector tubes, the mathematical model developed by Lugo-Granados and Picon-Nuñez (2017) is implemented. Through this model, it is possible to understand the effects of scaling fouling on the thermal and hydraulic performance of solar collectors, Eq(16).

$$\dot{m}_d = \frac{\beta}{2}\left(\frac{\beta}{\alpha\, k_r} + (C_1 + C_2) - \sqrt{\frac{[\beta + (C_{1+}C_2)\,\alpha\, k_r]^2 + 4\,\alpha^2\, {k_r}^2\left(K_{sp} - [C_1][C_2]\right)}{\alpha^2\, {k_r}^2}}\right) \tag{16}$$

The model determines the mass flow rate $\dot{m}_d$ (kg/m² s) of $CaCO_3$ deposited on the tubes (scaling formation) based on parameters such as pH, the concentration of Ca^{2+} (C1) (kg/m³), CO_3^{2-} (C2) (kg/m³), and the solubility constant (Ksp) (kg²/m⁶) of CaO_3 in water. The model incorporates the chemical reaction rate for crystal formation (kr, m²/(kg s)). The mass transfer coefficient β (m/s) is also included. Deposition resistance factor α (Eq(17)), is an experimental and dimensionless parameter dependent on viscous and inertial stresses. The thickness generated by scaling can be determined to by Eq(18).

$$\alpha = \frac{191}{f \cdot Re^{1.67}} \tag{17}$$

$$x_f = R_s \lambda_f \tag{18}$$

The overall efficiency (η_t) can be evaluated from Eq(19):

$$\eta_f = \frac{\dot{Q}_u}{I_G A_s} \tag{19}$$

From Eq(20), the pressure drop within the collector network can be calculated, which is proportional to the sum of hydraulic resistances K_i (kPa s²/m⁶) and the square of volumetric flow rate $\dot{V}$ (m³/s).

$$\Delta P_T = \dot{V}^2 \sum_{i=1}^{n} K \tag{20}$$

$$K_1 = \frac{8 L_t}{\pi^2 {d_s}^5} f \tag{21}$$

$$K_2 = \frac{8\rho}{\pi^2 {d_s}^4} k_f \tag{22}$$

Eq(21) and Eq(22) illustrate the primary hydraulic resistances. The frictional resistance K_1 (kPa s²/m⁶) is due to pipe length, and the loss coefficient resistance K_2 (kPa s²/m⁶) includes components such as elbows, valves, etc. Where f is the friction, k_f is the loss coefficient for fittings, L_t (m) and d_s (m) are the length and hydraulic diameter of the tube.

3. Thermal model validation

Experimental data from Gao et al. (2020) were used to validate the model. Figure 2(a) shows the experimental data (blue points) and the theoretical results (black line). It is observed that the theoretical results are very close to the experimental ones, with a maximum error of 2 % as shown in Figure 2(b). These results demonstrate the accuracy of the thermal model.

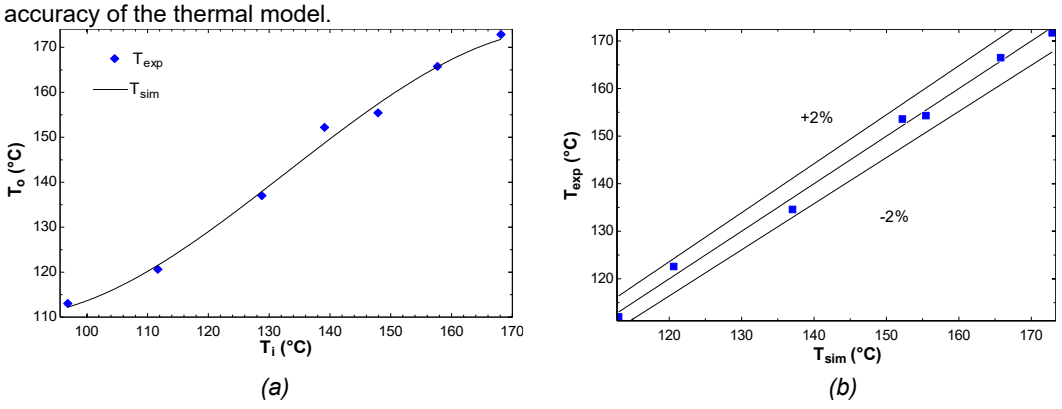

Figure 2: Comparison of the experimental and simulation results: a) outlet temperature vs. inlet temperature, b) error between predicted and measured outlet temperature

4. Results

In this study, a solar collector network was designed with the goal of reaching a temperature of 90 °C at 9:00 a.m. For this calculation, a solar radiation level of 688 W/m² was considered in the city of Zacatecas (Mexico) on a typical summer day, with a total flow rate of 80 l/min and an inlet temperature of 25 °C. The number of collectors connected in series per line required to achieve the target temperature (90 °C) depends on both the total flow rate (80 L/min) of the system and the total number of lines in the network. In this analysis, two network configurations were considered: one with 20 lines and another with 16 lines. The flow velocity was 0.12 m/s per collector for the first configuration and 0.15 m/s for the s. The operational performance of the plant was analysed over 5,040 h. The results showed that significant variations occurred every 720 h (every two months). Figure 2a displays the points where these effects were examined. Also, Figure 3a shows that, under initial conditions (without fouling), a network of 340 collectors is needed to reach 90 °C with a flow velocity of 0.12 m/s. This network was configured with 20 lines and 17 collectors connected in series per line. For a flow velocity of 0.15 m/s (16 lines), 21 collectors in series per line are required, resulting in a total of 336 collectors.

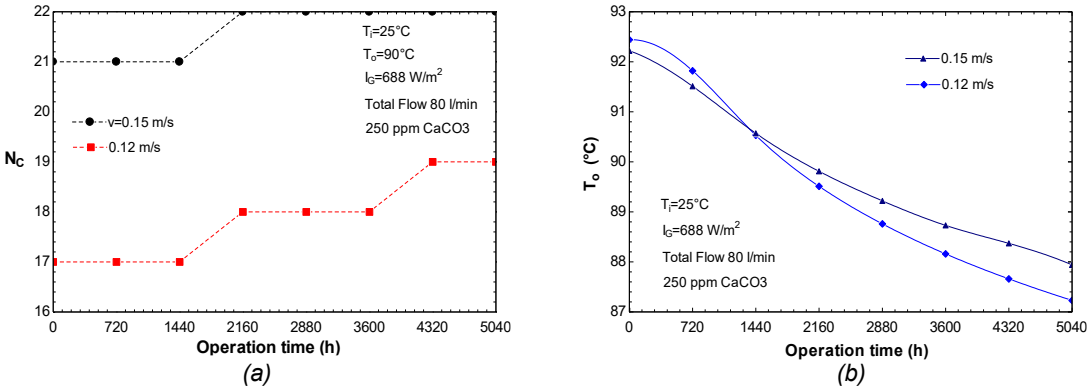

Figure 3: Thermal performance degradation as fouling builds up over time for different flow velocities: a) Number of collectors required, b) Outlet temperature

As operational time increases, fouling due to scaling inside the solar collectors reduces heat transfer. This necessitates increasing the number of collectors required to reach the target temperature. After 5,040 h of operation, with a flow velocity of 0.12 m/s, two additional collectors per line are needed, resulting in a total of 380 collectors in the network. For a flow velocity of 0.15 m/s, one additional collector per line is required after the same operation time, bringing the total to 352 collectors. Figure 3b shows the evolution of the outlet temperature (To) in the solar collector network as a function of operating time for two flow velocities: 0.12 m/s (blue line) and 0.15 m/s (black line). Over time, the temperature progressively decreases, along with a reduction in heat transfer and thermal efficiency of the system, all due to fouling caused by scaling. The temperature drop is more pronounced at 0.12 m/s, indicating that lower flow velocity promotes deposit accumulation and accelerates efficiency loss. After 5,040 h of operation, the outlet temperature significantly decreases in both configurations. In the network with a flow velocity of 0.15 m/s, the temperature reduction is 4.28 °C, while at a flow velocity of 0.12 m/s, the decrease reaches 5.21 °C. This confirms that higher flow rates help mitigate the adverse effects of scaling. Figure 4a presents the thermal efficiency profiles (ηf) of a solar collector network as a function of outlet temperature (To) for various operating times, considering the presence of fouling. It is observed that in all cases, thermal efficiency decreases as the outlet temperature increases. This is because higher temperatures result in increased thermal losses, reducing the system's capacity to transfer heat efficiently. The efficiency curve without fouling shows the best performance, while as time progresses (from 720 h to 5,040 h), the curves shift towards lower efficiency values. This indicates that the accumulation of scaling reduces heat transfer capacity, negatively affecting the system performance. The curves in Figure 4b show the pressure drop (ΔP) as a function of the number of solar collectors connected in series (Nc) for different operating times, considering the presence of fouling. The pressure drops increase as the number of solar collectors connected in series rises, due to the greater hydraulic resistance to flow. The pressure drops profiles shown in Figure 3b, for up to 10 collectors connected in series, were very similar across different operating times. However, for configurations with more than 15 collectors in series, the difference between the pressure drop profiles reaches up to 6,000 kPa.

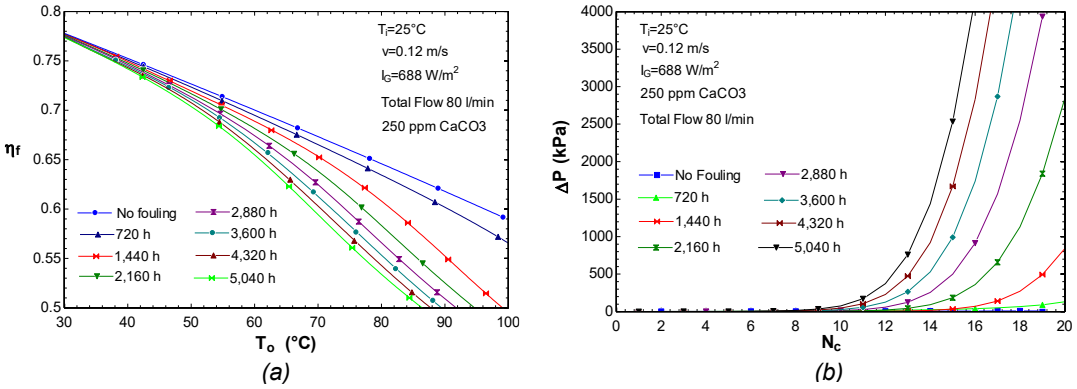

Figure 4: Performance variation due to fouling accumulation at different stages of operation: a) Efficiency vs. Outlet temperature, b) Pressure drop against number of collectors in series

As operating time increases, the pressure drop increases considerably because of the scaling impact in networks with more than 15 collectors arranged in series. The reference curve ("No Fouling") indicates the lowest pressure drop, suggesting an unrestricted flow. However, after 2,160 h, the pressure drop reaches extremely high values, indicating severe blockage in the ducts caused by the accumulation of deposits.

5. Conclusions

The presence of scaling gradually reduces thermal efficiency, necessitating a larger number of collectors to maintain the desired outlet temperature. At a flow velocity of 0.15 m/s, 21 collectors in series are required to reach the target temperature under clean conditions, whereas with scaling, this number increases to 22. On the other hand, at a flow velocity of 0.12 m/s, the system requires 17 collectors under clean conditions, but with fouling, it increases to 19. The results reveal that the pressure drop in the solar collector network increases significantly, especially when more than 10 collectors are connected in series and operating times exceed 2,160 h. This affects system performance and can increase pumping costs, highlighting the importance of mitigation strategies such as periodic cleaning or water treatment. The water flow velocity within the system directly influences the fouling rate: a higher flow velocity (0.15 m/s) helps mitigate its impact, and a lower flow velocity (0.12 m/s) accelerates the decrease in outlet temperature. However, it is important to consider that higher flow velocity leads to greater pressure drops, which increases pumping costs. Therefore, a network design with proper flow distribution not only improves system efficiency but also contributes to reducing operational costs and extending its lifespan.

References

Albizzati E., 2016, Sustainability assessment of solar installations with flat plate and evacuated tube collectors. International Journal of Environmental Pollution, 32, 315-322.

Bellos E., Tzivanidis C., 2023, A detailed investigation of an evacuated flat plate solar collector. Applied Thermal Engineering, 234, 121334.

Carrión-Chamba W., Murillo-Torres W., Montero-Izquierdo A., 2022, A review of the state-of-the-art of solar thermal collectors applied in the industry. INGENIUS, 27, 59-73.

Gao D., Gao G., Cao J., Zhong S., Ren X., Dabwan Y. N., Hu M., Jiao D., Kwan T. H., Pei G., 2020, Experimental and numerical analysis of an efficiently optimized evacuated flat plate solar collector under medium temperature. Applied Energy, 269, 115129.

Haghverdi K., Martinopoulos G., Misirlis D., 2023, Fluid Flow and Heat Transfer CFD Analysis Inside Solar Flat Plate Collectors. Chemical Engineering Transactions, 103, 457-462.

Lugo-Granados H., Picón-Núñez M., 2017, Scaling Growth in Heat Transfer Surfaces and Its Thermohydraulic Effect Upon the Performance of Cooling Systems. Chemical Engineering Transactions. 103, 421-426.

Lugo-Granados H., Canizalez-Dávalos L., Picón-Núñez M., 2023, Thermohydraulic Effects of Scaling in Flat Plate Solar Collector Networks. Chemical Engineering Transactions, 103, 421-426.

Lugo-Granados H.G., Picón-Núñez M., Canizalez-Dávalos L., 2024, Flat plate solar collector networks: Design and retrofit considering fouling effects. Thermal Science and Engineering Progress, 51, 102633.

Nedunchezhiyan M., Ramalingam S., Natesan P., Sampath S., 2025, CFD-Based Optimization of Solar Water Heating Systems: Integrating Evacuated Tube and Flat Plate Collectors for Enhanced Efficiency. Case Studies in Thermal Engineering, 69, 106017.